Single charge transport standards and quantum-metrological triangle experiments

F. Piquemal, L. Devoille, N. Feltin and B. Steck

Laboratoire National de Métrologie et d'Essais LNE - Trappes F 78197, France

1. – Introduction

In the present Système International d'Unités SI, the link between electrical and mechanical units is made through a realisation of ampere [1]. However, the direct determination of ampere cannot be carried out with a sufficient accuracy. In practice, it is more relevant to realise first the derivative electrical units, on the one hand farad and ohm, on the other hand volt (fig. 1). That allows the determination of ampere afterwards with a better uncertainty. The farad occupies a special place in the realisation of electrical units by means of a Thompson-Lampard calculable capacitor [2]. The setting-up of this calculable capacitor makes the SI realisation of the ohm possible through a comparison between impedances of capacitor and resistor [3]. That leads to a determination of the von Klitzing constant R_{K} originated from the quantum Hall effect (QHE) [4-6]. This effect links a resistance to a fundamental constant as the ac Josephson effect (JE) [6, 7] links electromotive force to another fundamental constant, the Josephson constant K_{J}. Furthermore the theory predicts that $R_{\mathrm{K}} = h/e^2$ and $K_{\mathrm{J}} = 2e/h$.

These two quantum phenomena have a great impact in metrology because firstly they provide fundamental standards with reproducible values independent of space and time, getting unique the representation of the ohm and the volt. Secondly, through SI realisation of electrical units, QHE and JE contribute significantly in the improvement of the knowledge of constants of nature [8]. For instance, the SI realisations of the ohm and the watt balance experiments [9, 10] lead to determine the well-known fine-structure constant $\alpha = \mu_0 c/(2h/e^2)$ and the Planck constant if one assumes that QHE and JE give h/e^2 and $2e/h$ exactly.

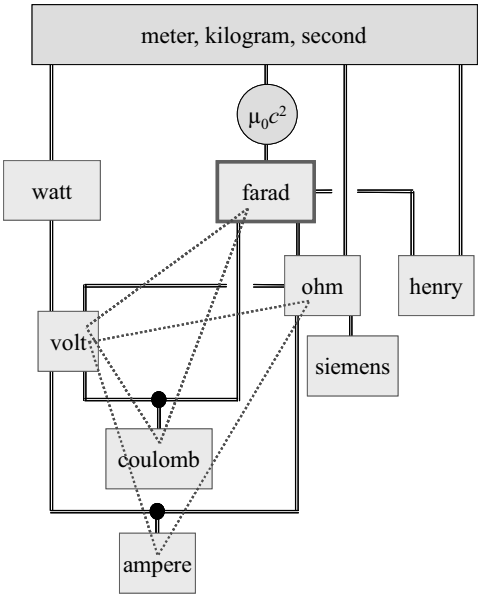

Fig. 1. – Chain of SI realisations of electrical units and metrological triangles. According to the present definition of ampere, the value of the permeability of vacuum μ_0 is fixed: $\mu_0 = 4\pi \times 10^{-7}\,\mathrm{N/A^2}$. The value of the speed of light in vacuum being fixed for the definition of the meter, leads to conventionally exact values of the permittivity of vacuum $\varepsilon_0 = 1/\mu_0 c^2$ ($\approx 113\,\mathrm{pF/m}$) and the free-space impedance $Z_0 = (\mu_0/\varepsilon_0)^{1/2}$ ($\approx 377\,\Omega$).

The paper deals with a third quantum phenomenon, the Single Electron Tunnelling (SET), and its main applications that could disrupt again the electrical metrology. This phenomenon indeed makes the development of quantum standard of current possible whose amplitude is directly linked to the elementary charge. The Quantum Metrological Triangle (QMT) experiment originally suggested by Likharev and Zorin [11] enables to test directly the coherence of the constants involved in QHE, JE and SET phenomena which are strongly presumed to provide the free-space values of h/e^2, $2e/h$ and e. This experiment consists either in applying Ohm's law $U = RI$ or in following $Q = CU$ [12] from the realisation of an electron counting capacitance standard [13]. Moreover combining QMT with watt balance and Thompson-Lampard calculable capacitor will lead to a determination of the elementary charge. These issues point out the important role that SET experiments should play toward the foundation of new SI system fully based on fundamental constants, for example by fixing h and e for a redefinition of the kilogram and the ampere([1]).

([1]) Other competitive proposals are to fix Avogadro number N_A instead of h for a new definition of the unit of mass and to keep μ_0 fixed for a reformulation of the ampere and the electrical units putting forward the free-space impedance Z_0.

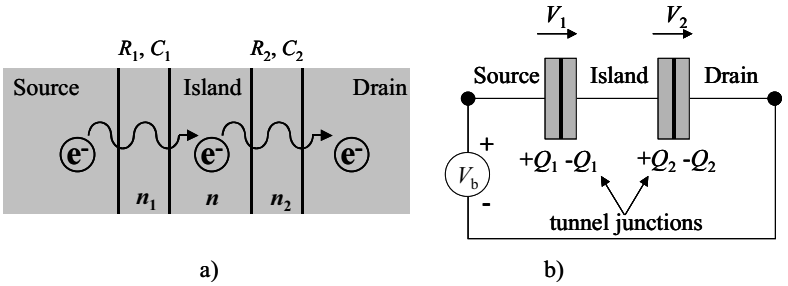

Fig. 2. – a) Schematic representation of a double tunnel junction. R_j is the tunnel resistance and C_j the junction capacitance. b) Symbolic representation of the circuit.

Section **2** describes basic theoretical elements on single electron tunnelling devices from double tunnel junctions to electron pump. For a detailed description on the theory, the reader is referred to review articles [14-16]. Section **3** deals with other single charge transport devices. Section **4** mainly covers the metrological triangle experiments and their impacts for fundamental constants. Conclusions and prospects are given in sect. **5**.

2. – Single electron devices

2˙1. *The elementary device based on Coulomb blockade*. – The Coulomb blockade of electron tunnelling, observed for the first time in disorder granular materials [17], appears when a part of a circuit, named "island", is electrically isolated from the rest of the circuit due to two tunnel junctions. On fig. 2, n_1 (respectively, n_2) is defined as the number of electrons which can be transferred through the first (respectively, the second) junction and n is the number of excess electrons on the island: $n = n_1 - n_2$. The charges Q_1 and Q_2 on the electrodes of capacitances C_1 and C_2 are continuous variables. n denotes the excess charge on the metallic island and changes only with a tunnel event inducing the entrance or the exit of an electron of the island. It leads to a quantization of the island charge and this feature is the cause of the single-electron effect in these systems.

Let us consider the circuit on fig. 2 b). A bias voltage source V_b is added to the double junction described on fig. 2 a). When this circuit is not voltage biased ($V_\mathrm{b} = 0$), there is no excess electron on the island. The island is strictly neutral in charge. On contrary, an applied voltage ($V_\mathrm{b} \neq 0$) will lead to a tunnel transfer through one of the junctions and to the presence of excess charges on the island. This charge variation is necessarily discrete as demonstrated below.

The electron transfer through a double tunnel junction can be treated from thermodynamics. The variation of Helmholtz free energy is defined as the difference between the electrostatic energy stored in the device described on fig. 1 and the work supplied by the voltage source V_b. This energy variation is

$$\Delta F = \Delta E_\mathrm{C} - \Delta W. \tag{1}$$

From a phenomenological point of view, the system will tend to minimize the free energy by means of tunnel transfers. The charge on the island can be written as

$$Q = Q_2 - Q_1 = -ne. \tag{2}$$

By assuming for each junction that, on the one hand, the system has time to energetically relax between two tunnel events, and on the other hand, the charge transfers are fast enough, the variation of free energy of each junction can be calculated. The basic idea is to express the voltages V_1 and V_2 across each junction, in order to calculate the electrostatic energy and the work of the sources. The voltage at each junction terminal is

$$V_1 = (-C_2 V_\mathrm{b} + ne)/C_\Sigma, \tag{3}$$

$$V_2 = (-C_1 V_\mathrm{b} - ne)/C_\Sigma \tag{4}$$

with $C_\Sigma = C_1 + C_2$. Moreover, the electrostatic energy stored by both junctions is

$$E_\mathrm{C} = {Q_1}^2/2C_1 + {Q_2}^2/2C_2 = \left[{V_\mathrm{b}}^2 C_1 C_2 + (ne)^2\right]/2C_\Sigma. \tag{5}$$

To get the free energy, the work of the source has to be calculated. If one electron crosses the first junction, the charges on the island and on the right (${Q_1}^-$) and left (${Q_1}^+$) electrodes of the first junction will be changed. It will lead to an electrostatic unbalance and the source will have to oppose to the voltage change due to the tunneling event. During this charge transfer the voltage V_1 varies by a quantity $-e/C_\Sigma$ corresponding to a charge $-eC_1/C_\Sigma$. But, in order to reach the electrostatic balance, the voltage source V_b has to bring the total polarization charge $-eC_2/C_\Sigma$. The work inherent to the transfer of n_1 electrons through the first junction and then of n_2 electrons through the second one becomes

$$W_1 = -n_1 e V_\mathrm{b} C_2/C_\Sigma, \tag{6}$$

$$W_2 = -n_2 e V_\mathrm{b} C_1/C_\Sigma. \tag{7}$$

Consequently, the tunnel event of one electron in one of the both directions through the first or the second junction leads to the free-energy variation $\Delta F = \Delta E_\mathrm{C} - \Delta W$

$$\Delta {F_1}^\pm = F(n_1 \pm 1, n_2) - F(n_1, n_2) = (e/C_\Sigma)[e/2 \pm (V_\mathrm{b} C_2 + ne)] = e^2/2C_\Sigma \pm eV_1, \tag{8}$$

$$\Delta {F_2}^\pm = F(n_1, n_2 \pm 1) - F(n_1, n_2) = (e/C_\Sigma)[e/2 \pm (V_\mathrm{b} C_1 - ne)] = e^2/2C_\Sigma \pm eV_2. \tag{9}$$

To make a charge transfer possible through the double junction, a negative free-energy variation is needed. From previous expressions, the condition on the bias voltage (by assuming no excess charge on the island, $n = 0$) leads to the appearance of a threshold voltage V_t given by

$$|V_\mathrm{b}| \geq V_\mathrm{t} = e/C_\Sigma. \tag{10}$$

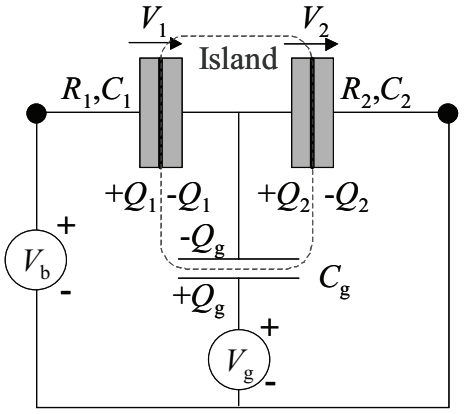

Fig. 3. – Schematic view of a SET transistor.

As long as the condition (10) is not fulfilled, no electron can be transferred, the current is blocked. This phenomenon, based on Coulomb repulsion, is named Coulomb blockade. The addition of one charge generates an electric field E which can stop the tunnel transfer of an excess electron through the first junction. $e^2/2C_\Sigma$ is the energy associated to the Coulomb blockade and this energy is in the first term of eqs. (8), (9). This expression reminds the purely classical model of electron-electron interaction based on the capacitive charge energy defined by Coulomb.

2˙2. *The single-electron transistor*. – In the previous section the principle of Coulomb blockade has been presented for an elementary device: two tunnel junctions in series. In this part let us introduce the SET transistor schematised in fig. 3. A gate electrode of capacitance C_g coupled to the island has been added in order to change the charge state of the island. Thus the number of charges on the island can be controlled by means of the gate voltage and the charge can be written as

$$Q_2 - Q_1 = -ne - C_\mathrm{g}(V_\mathrm{g} + V_2). \tag{11}$$

Note that a voltage offset applied to this additional gate electrode can compensate for the effects due to background charges coming from impurities or vacancies. From the relations (8) and (9) and with taking the energy stored by the gate capacitor into account, the free-energy changes during a tunnel event through the first or the second junction become

$$\Delta {F_1}^{\pm} = e^2/2C_\Sigma \pm eV_1 = (e/C_\Sigma)\big[e/2 \pm \big(- \big(C_2 + C_\mathrm{g}\big)V_\mathrm{b} + C_\mathrm{g}V_\mathrm{g} - ne\big)\big], \tag{12}$$

$$\Delta {F_2}^{\pm} = e^2/2C_\Sigma \pm eV_2 = (e/C_\Sigma)\big[e/2 \pm \big(- C_1V_\mathrm{b} - C_\mathrm{g}V_\mathrm{g} - ne\big)\big] \tag{13}$$

with $C_\Sigma = C_1 + C_2 + C_\mathrm{g}$.

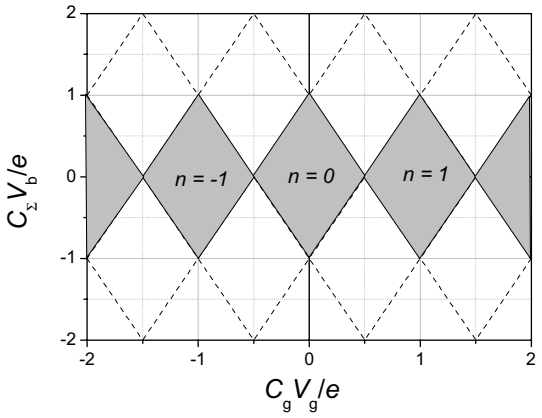

Fig. 4. – Stability diagram of a single-electron transistor showing the blocked (grey) and open (white) state domains.

As previously mentioned a tunnel event occurs only if it involves a decrease of the free energy. As a result, from inequalities $\Delta {F_1}^{\pm} \leq 0$, $\Delta {F_2}^{\pm} \leq 0$ and relations (12), (13), a stability diagram can be constructed. Such a diagram with a diamond shape allows us to display the Coulomb blockade regions in the $V_\mathrm{b} \otimes V_\mathrm{g}$ plane (fig. 4).

The grey regions correspond to stability domains with an integer number of excess electrons on the island. The probability of transmission through the barrier is very low, the current intensity is zero and the device is in the so-called blockade state. Everywhere else the transistor is in an open state and in this case the tunnelling of electrons through the circuit is possible. Note that at finite bias voltage below the threshold value $|V_\mathrm{t}| = e/C_\Sigma$ given in (10) the current oscillates with a period e/C_g with increasing gate voltage. Therefore the gate capacitance C_g can be estimated from the diamond diagram. Above $|V_\mathrm{t}|$ any Coulomb blockade does not arise. Whatever the voltage applied to gate electrode is, the current intensity is non-zero.

In order to well understand the origin of Coulomb blockade, let us refer to the energy band diagram sketched in fig. 5.

The Coulomb electrostatic energy $e^2/2C_\Sigma$ derived from the formulas (8) and (9) involves an energy band gap e^2/C_Σ shown in fig. 5a. The energy level denoted E_{n+1} corresponding to a single excess electron within the island is above the Fermi source energy, which makes an electron tunnelling from the left electrode impossible. The device is in a blockade state and the current is zero: this is the Coulomb blockade. Applying a voltage V_g to the gate electrode induces the lowering of the island energy levels (Fermi energy and E_{n+1}). Therefore E_{n+1} ends up being sandwiched between the both electrodes energy level in fig. 5b. As a result the electrons can cross the transistor from the source to the drain. Note that a similar situation can be achieved with increasing the bias voltage V_b. Each excess electron on the island tunnelling through the second junction leads to a drop in the energy to E_n which allows a second electron to penetrate into the island.

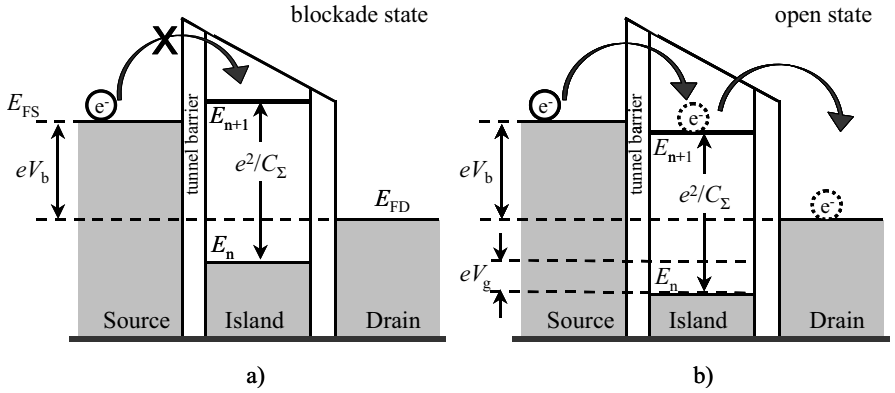

Fig. 5. – Energy band diagram before (a) and after (b) changing gate voltage. $E_{F,S}$, E_n and $E_{F,D}$ denotes the Fermi energy level of the source, island and drain, respectively. The gap between the source and drain energy levels is due to the bias voltage. n represents the free-electron number contained within island before tunnelling.

Finally, the Coulomb blockade phenomenon is illustrated by the measurements given in fig. 6. On the left picture the charge effects involve periodical changes of the transport properties with the gate voltage V_g. The period corresponds to an addition of one electron to the island. V_g can be adjusted so that the electron transfer through the device is blocked and so the current is zero. Consequently, the current can be suppressed thanks to two parameters: V_g and V_b. Below the threshold voltage no electron can tunnel and the current is zero as observed in fig. 6 right.

In this part we have described a device making the transfer of electrons one by one possible. However, a SET transistor is not capable of controlling the electron flow and so the current intensity. Designing a quantum current standard implies a more complex system than a SET transistor as described in the next part.

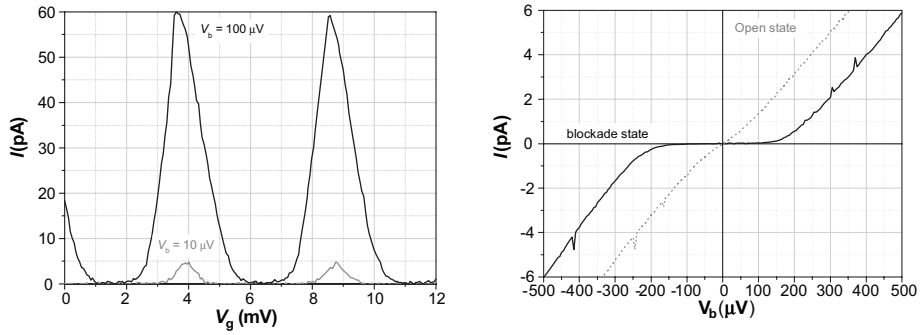

Fig. 6. – I-V characteristics of a SET transistor. Left: Coulomb oscillations obtained with varying gate voltage at various bias voltage. Right: I-V_b curve measured in the blockade and open states.

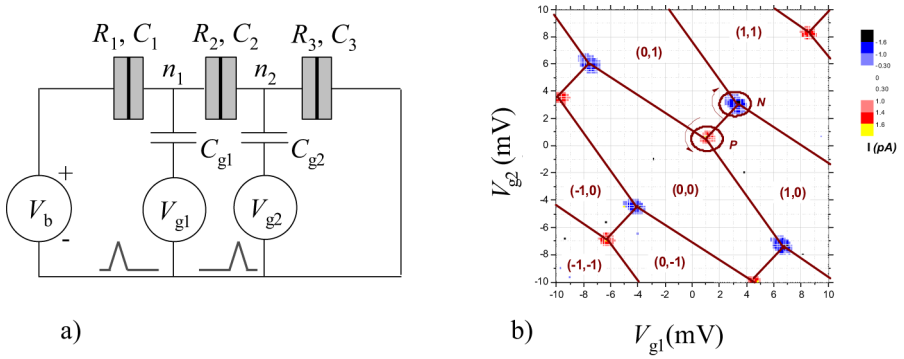

Fig. 7. – a) Schematic view of 3-junctions pump. b) Stability diagram in $V_{g1} \otimes V_{g2}$ plane which displays the stable configurations (n_1, n_2) of numbers of the excess electrons on each island. A RF signal at 10 MHz is applied to the gates. Boundaries between the domains (full lines) form a typical honeycomb pattern. The charges tunneling transfer takes place only in the triple points. These measurements have been carried out at LNE by means of a CCC used as a current amplifier.

2˙3. *The electron pump.* – The SET pump, first investigated by Pothier *et al.* [18] is a device allowing the transfer of electrons one by one at an adjustable clock frequency, f, and of a quasi-adiabatic way. Therefore, the electric current through the electron pump can be expressed by: $I = e \cdot f$. The simplest electron pump consists of two metallic islands separated by three junctions (ideally $C_1 = C_2 = C_3$, typically 150–200 aF). The gate voltages V_{g1} and V_{g2} through the gate capacitance C_{g1} and C_{g2} (typically around few tens of aF) can control the electric potential of each island (fig. 7a). The pump operation can be illustrated by means of the typical diagram given in fig. 7b which displays the stability domains of the different states (n_1, n_2) in the $V_{g1} \otimes V_{g2}$ plane.

The integer couple (n_1, n_2) denotes the number of excess charges located on the first and the second island respectively. The points (fig. 7b), so-called triple points, where conduction can take place, share three neighbouring domains. Everywhere else, the pump is in a blockade state and the electron configuration (n_1, n_2) is stable. Lines represent the boundaries between each stability domains and form a typical honeycomb pattern. The pumping of electrons is based on these topological properties.

The controlled transfer of electrons is obtained in the following way: two periodic signals with the same frequency f but phase shifted by $\Phi \approx 90°$ are superimposed on each applied d.c. gate voltage couple (V_{g10}, V_{g20}) as follows:

$$V_{g1} = V_{g10} + A \cdot \cos(2\pi \cdot f \cdot t),$$
$$V_{g2} = V_{g20} + A \cdot \cos(2\pi \cdot f \cdot t + \Phi).$$

In case the d.c. voltages (V_{g10}, V_{g20}) correspond to coordinates of the point denoted P, the circuit follows a closed trajectory around P as shown in fig. 7b. The

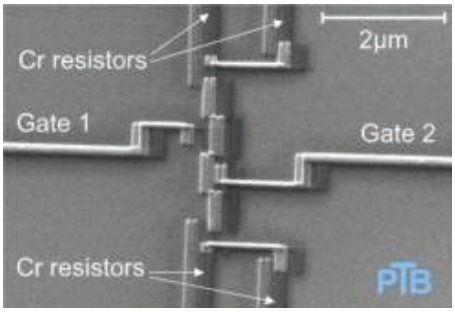

Fig. 8. – SEM-image of a 3-junctions R pump fabricated by PTB [23] (illustration by courtesy of PTB).

configuration changes from (0,0) to (1,0), then from (1,0) to (0,1), and returns to the initial state (0,0). In the real space, the complete sequence involves the transfer of one electron throughout the pump.

The frequency has to be lower than the reciprocal of the tunnel rate ($f \ll R_{\mathrm{j}}C$, R_{j} is the junction resistance, typically around 100–150 kΩ). This condition ensures that the system adiabatically returns to its ground state. By adding 180° to the phase shift Φ, the rotation sense is reversed in configuration space, and the electron by electron current takes place in the opposite direction [19]. The honeycomb pattern depends on gates and junctions capacitances and on cross-capacitances between the first gate electrode and the second island and *vice versa*. This effect can be compensated by means of an electronic device connected to both gate wiring inputs which adds a fraction of the voltage applied to one gate to the other gate, with opposite polarity [20].

The accuracy of the charge transfer is limited by three phenomena: thermal errors, frequency errors and co-tunneling effect [21]. The co-tunnelling effect is the most constringent one. This phenomenon involves simultaneous tunnelling of electrons from islands through each junction. In order to avoid errors in the transport rate, a first solution is the increase of the number of junctions. NIST has demonstrated that an error rate at a level of one part in 10^8 or less has been reached with a 7-junctions pump [22]. But, instead of it, PTB has proposed to keep 3-junctions pumps, the easiest to use, and to place on-chip resistive Cr-micro strips of typically 50 kΩ in series with the pump [19, 23], thus named R-pump (fig. 8). As a result, the dissipation of electron tunnelling energy in the resistors suppresses undesirable effects of co-tunnelling([2]) and an increased accuracy can be achieved.

In fig. 9 a set of I-V_{b} curves, named current steps, are shown and illustrates the quantization and the stability of the current generated by a R-pump with bias conditions at various frequencies. These characteristics are determining for the development of

([2]) A 3-junctions pump with a total Cr resistance of 50 kΩ is roughly equivalent, for co-tunneling, to a 5-junctions pump [23].

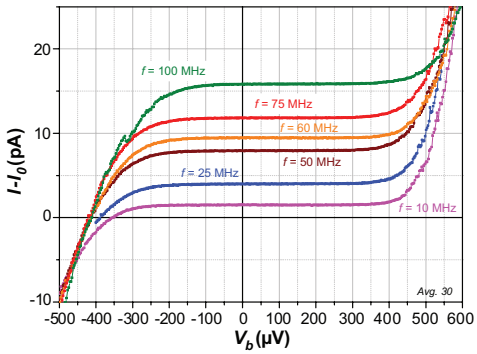

Fig. 9. – Current steps measured with a PTB R-pump operating at various pumping frequencies and at $T_{\mathrm{bath}} = 50\,\mathrm{mK}$.

current standards. Thus, stable current on $300\,\mu\mathrm{V}$ in a 40 fA range was obtained with a PTB R-pump connected to a CCC [24]. An investigation on long time measurements has shown that these pumps were able to generate a quantified current during more than 12 hours [19].

3. – Other single charge transport devices

3˙1. *RF-SET-transistor–based electron counter*. – The bandwidth of a classical SET transistor used as an electrometer is typically around 1 kHz and can achieve 1 MHz with some improvements. But, it is too low to detect a 1pA current with a metrological accuracy, which requires a bandwidth of 10 MHz at least. Therefore, following the principle of the RF SQUID technology, a SET transistor is embedded in a tank circuit. Such a device, called RF-SET, can reach a charge resolution six orders of magnitude better than the commercial conventional detectors, the best result reported so far being $1.10^{-6}\,e/\mathrm{Hz}^{-1/2}$ [25].

The RF-SET is capacitively coupled to a long array of tunnel junctions, makes the electrons counting one-by-one possible (fig. 10) [26]. In a long array of tunnel junctions, charges flow in the form of regularly spaced solitons. Electrons generated by an external current source penetrate into the array of junctions and change the charging state of the island of the transistor when they come close to it. An incident RF signal is partially absorbed by the RF-SET if the transistor is in the open state or totally reflected in the blockade state. Consequently, this system is able to detect the crossing of an individual electron by counting each change of state. In principle, the aim should be to reach a counting speed of at least 60 MHz, corresponding to 10 pA with a 10 parts in 10^6 uncertainty. However, the best measurements reported so far show measured current less than 1 pA [27].

3˙2. *SETSAW pump*. – The principle and the design of the electron transfer using a surface acoustic wave (SAW) generating a quantized current is quite different from the

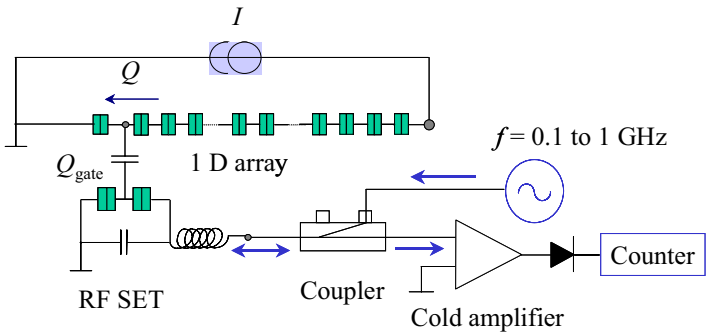

Fig. 10. – Basic circuit of an RF-SET electrometer. I is calibrated in terms of e and f by measuring the average frequency of the signal caused by the time correlated SET oscillations in 1D array.

one of the pumps, but the SETSAW devices remain interesting candidates for developing a current standard source or for quantum computing. A 2DEG in a heterostructure of GaAs/AlGaAs, very similar to those present within QHE devices, is confined to a one-dimensional (1D) channel by using split-gate technique (fig. 11). Thus, this channel is located between two electron reservoirs. By applying an appropriate voltage to the gate, the electron density in the constriction can be reduced to zero and an energy barrier for electrons appears. Due to the piezoelectric effect, a potential modulation is created, propagates through the SETSAW and is superposed to the energy barrier in the constriction area. Based on the Coulomb repulsion, it has been shown that an integer number of electrons, determined by the created well size, can be transferred through a SETSAW device and generates a current $I = N \cdot e \cdot f$ [28]. The maximum speed would be around 10 GHz.

For several years, the collaboration between the University of Cambridge and NPL has extensively investigated and developed a SETSAW current standard [29]. A total

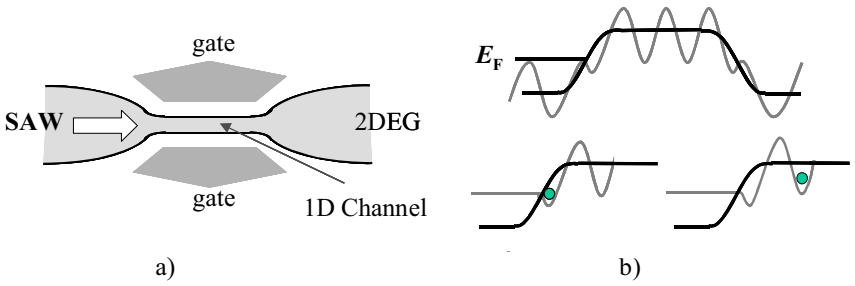

Fig. 11. – a) Schematic of the active part of a SETSAW device. b) Superposition of the surface acoustic wave and the barrier created by the split gates. The Fermi level of the 2DEG is indicated. The hollows of the modulation of the energy act like potential well which can propagate a single electron through the barrier.

current uncertainty of a few parts in 10^4 has been estimated but no real flat plateau has been displayed [30]. This lack of accuracy would no more ascribed to the overheating of electrons due to RF power needed by the transducer and by the speed of switching on and off of the propagating acoustic wave but would be explained by impurity effects [31]. From a model based on Coulomb blockade and a quantum dot within the 1D channel, it has been found that a current quantization $I = ef$ may occur at low RF power when SAW amplitude corresponds to a quantum dot charging energy and at gate voltage slightly exceeding the threshold value above which the channel is depleted. This single electron transport is maintained close to equilibrium, *i.e.* with limited overheating of electrons [31, 32]. We note ongoing developments of SETSAW pump based on carbon nanotubes [33, 34].

3˙3. *Cooper pair pump.* – In principle, the devices consisting of small-capacitance Josephson junctions forming superconducting islands coupled to gate electrodes are able to pump Cooper pairs one-by-one driven by a frequency higher than in the *normal* pump case. However, the tunnelling of cooper pairs is a phenomenon more complex than the one of electrons in the normal state because the Josephson coupling energy, E_J ($= hI_\mathrm{C}/(4\pi e)$ where I_C is the critical current of the Josephson junction) must be taken into account and compared directly to the charging energy, E_c. Nevertheless, with $E_\mathrm{J} < E_\mathrm{c}$, a current $I = \pm 2ef$ generated by a three-junction superconducting pump has been observed by several authors [14, 35, 36]. But, the transfer of the Cooper pairs across the device is disturbed by factors (Cooper pair co-tunnelling, quasi-particles poisoning ...) involving an imperfect plateau of the I-V curve. In order to improve the accuracy of the superconducting pumps, Zorin *et al.* have proposed to connect resistors in series to the ends of the array following the example of their R-type normal pumps [36]. The measurements show the through-supercurrent and the unwanted co-tunnelling events are dramatically suppressed.

3˙4. *New devices.* – Another approach to pump single Cooper pairs per cycle has been proposed by Niskanen *et al.* The device, referred to as Cooper pair sluice, consists of two mesoscopic SQUIDs forming between them a superconducting island, which is fitted with a gate [37, 38]. The gate provides the possibility of coherent transfer of Cooper pair charges, one at a time, under the influence of an applied RF signal. Quantized currents of 10 up to 100 pA could be obtained with a calculated accuracy of one part in 10^7.

Different particular Josephson devices are currently investigated for the observation of the Bloch oscillations (see, *e.g.*, [39-41]). These are periodic oscillations which manifest on the voltage across a current biased single Josephson junction at frequency $f = I/2e$ [11, 42]. The Bloch voltage oscillations and the Josephson current oscillations are actually dual phenomena. Phase locking Bloch oscillations by an external microwave signal could yield current steps in the I-V characteristics. Very recently, it has been shown that the current range of 100 pA–1 nA could be attainable [40]. Following the example of Josephson voltage standards, the Bloch oscillation devices are thus expected to be promising candidates for realising quantum current standards.

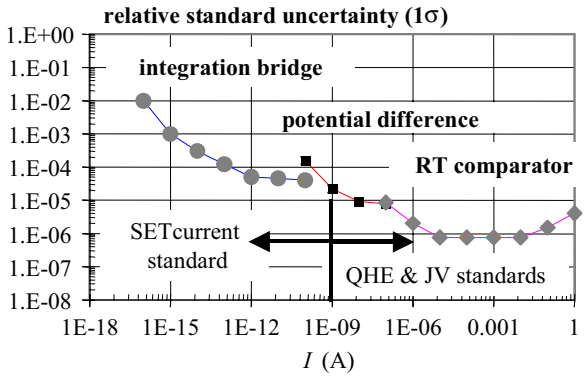

Fig. 12. – Different methods (current comparator at room temperature, potential difference bridge, integration bridge) used for the calibration of current less than 1 A and corresponding uncertainties. The integration method consists in the measurement of the rising time of the supplied current for a given voltage variation applied to a capacitance or inversely in the measurement of a varying voltage across a same capacitance along a known period.

To make up the list of single charge transport devices, we have to come back to non-superconducting devices and to mention the promising development of silicon-based SET pumps. The advantage of the silicon over aluminium lies not only in a possible higher pumping frequency (due to a smaller RC time constant), but also in a high stability of the background charge and a higher operating temperature ($T > 1\,\mathrm{K}$). First measurements on silicon-based SET pump with tuneable barriers have shown current steps at a level of 16 pA ($f = 100\,\mathrm{MHz}$) and at temperature as high as 20 K [43].

4. – New electrical standards and quantum metrological triangle experiments

4˙1. *Electrical standards.* – In practice, the ampere is reproduced by means of the ohm and the volt represented by the quantum Hall resistance standards (QHRS) and the Josephson array voltage standards (JAVS) respectively. On the other hand, the farad is reproduced by implementing a Thompson-Lampard calculable capacitor or by means of the QHRS associated to a measurement chain linking resistance to capacitance. However, the development of the Quantum-Metrological Triangle (QMT) experiments, which will be described below, requires quantum current or capacitance standards. SET devices are particularly well suited for these standards, which will play an important role for the "mise en pratique" of the possible redefinition of ampere and farad within the frame of a new SI to be implemented in mid term.

It is noteworthy that in shorter term the direct use of SET as primary current standard will be relevant for a current range less than 1 nA (fig. 12). This concerns the calibration of sub-nano ammeters (commercial electronic devices or home-made integration bridges) which allow national metrology institutes in electrical and ionising radiation domains to calibrate then their own secondary low-current standards and high-value resistance

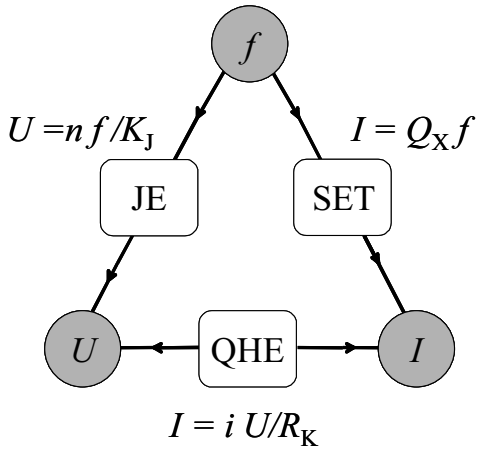

Fig. 13. – Quantum-metrological triangle. Theory predicts that R_{K}, K_{J} and Q_{X} correspond to the fundamental constants h/e^2, $2e/h$ and e.

standards ($R > 1\,\mathrm{T}\Omega$). The improvement of the traceability of small currents should benefit to some instrument manufacturers (detectors or meters of small electrical signals) and to the semiconductor industry (characterization of components, testing of wafers).

4˙2. *Quantum-Metrological Triangle.* – SET, or more widely, Single Charge Transport, provides the missing link of the Quantum-Metrological Triangle (QMT) (fig. 13) by realising a quantum current standard whose amplitude is only given by the product of the elementary charge by a frequency. The closure of the QMT experimentally consists here in applying Ohm's law $U = RI$ directly from the three phenomena SET, Josephson effect (JE) and Quantum Hall Effect (QHE). Another approach to close the triangle proposes to apply $Q = CV$ by means of a quantum capacitance standard.

In practice, the experiment amounts to determine the dimensionless product $R_{\mathrm{K}}K_{\mathrm{J}}Q_{\mathrm{X}}$, expected to be equal to 2, where the constant Q_{X} is defined as an estimate of the elementary charge [12], $Q_{\mathrm{X}} = e|_{\mathrm{SET}}$, by analogy with the definitions of Josephson and von Klitzing constants, $K_{\mathrm{J}} = 2e/h|_{\mathrm{JE}}$ and $R_{\mathrm{K}} = h/e^2|_{\mathrm{QHE}}$. Checking the equality $R_{\mathrm{K}}K_{\mathrm{J}}Q_{\mathrm{X}} = 2$ with an uncertainty of one part in 10^8 will be a relevant test of the validity of the three theories.

The experiments testing the universal character of JE and QHE by showing that the Josephson-voltage-frequency quotient V_{J}/f and the product index of the QHE plateau times the resistance of the plateau $i \times R_{\mathrm{H}}(i)$ are independent of materials at a level of parts in 10^{16} [44] and parts in 10^{10} [45,46], respectively, and the high level of agreement shown by numerous comparisons of quantum voltage and resistance standards (part in 10^{10} to a few parts in 10^9, respectively) ([6] and references therein) undoubtedly strengthen our confidence in the universal and fundamental aspects of K_{J} and R_{K} and hence in the equalities $K_{\mathrm{J}} = 2e/h$ and $R_{\mathrm{K}} = h/e^2$. However, even if strong theoretical arguments

exist, the high reproducibility of the JE and the QHE, from a strictly metrological point of view, does not prove these relations.

The validity of these two relations has been recently tested by the CODATA Task group in the framework of the 2002 fundamental constants adjustment. It is shown that there is no significant deviation between K_{J} and $2e/h$ and between R_{K} and h/e^2 but within a fairly large uncertainty in the case of Josephson relation. The uncertainties amount to 8.5 and 2 parts in 10^8, respectively [8]. Very recently, Mohr *et al.* noted opposite significant deviations of K_{J} from $2e/h$ when the data coming from X-ray Crystal Density (XCRD) measurement on Si sphere $V_{\mathrm{m}}(\mathrm{Si})$ or from gyromagnetic ratio measurements in low field $\Gamma'(\mathrm{lo})$ are alternatively deleted from the set of input data [47] $K_{\mathrm{J}}/(2e/h) = 1-(273\pm95)\times10^{-9}$ and $K_{\mathrm{J}}/(2e/h) = 1+(546\pm161)\times10^{-9}$, respectively.

These discrepancies (different by 8 parts in 10^7), which perhaps could be correlated to the present discrepancy of one part in 10^6 on the value of h, measured either by means of watt balance or through XCRD measurement, emphasize the usefulness to close the triangle even with an uncertainty level of few parts in 10^7.

4˙2.1. QMT by applying Ohm's law $U = RI$. The first way to close the QMT by applying Ohm's law on quantities provided by QHE, JE and SET consists in the direct comparison of the voltage U_{J} supplied by a Josephson junctions array to the Hall voltage of a QHE sample crossed by a current I delivered by a SET current source. The current is amplified with a high accuracy by means of a cryogenic current comparator (CCC) [12]. This comparison leads to the relation

$$U_{\mathrm{J}} = R_{\mathrm{H}} G I, \tag{14}$$

where G is the gain or winding ratio of the CCC. Considering the JE, QHE and SET relationships, eq. (14) becomes

$$n f_{\mathrm{J}}/K_{\mathrm{J}} = \big(R_{\mathrm{K}}/i\big) G Q_{\mathrm{X}} f_{\mathrm{SET}}, \tag{15}$$

where n is the index of the voltage step delivered by the JAVS at the microwave frequency f_{J}, i is the index of the QHE plateau and f_{SET} is the driving frequency of the SET current source. It leads to the dimensionless product

$$R_{\mathrm{K}} K_{\mathrm{J}} Q_{\mathrm{X}} = n(i/G) f_{\mathrm{J}}/f_{\mathrm{SET}}. \tag{16}$$

Another approach which leads to the same relation (16) consists in balancing the current delivred by the SET device against the current applied to a cryogenic resistor of high resistance value (100 MΩ) by a Josephson voltage. The current is detected by a CCC operating as an ammeter [48]. Then the same CCC is used for calibrating directly the 100 MΩ resistance with the quantum Hall resistance standard [49].

Measuring the deviation of $R_{\mathrm{K}} K_{\mathrm{J}} Q_{\mathrm{X}}$ from 2 will give information on the consistency level of the three quantum phenomena. It is noteworthy that the quantum charge involved

in SET will be determined in terms of the elementary charge e if one assume $R_K = h/e^2$ and $K_J = 2e/h$.

4˙2.2. QMT and electron counting capacitance standard. The development of a capacitance standard from SET devices, the so-called Electron Counting Capacitance Standard (ECCS), is feasible by applying the natural definition of the capacitance: the transfer of a well-known charge Q between the electrodes of a cryogenic capacitor with a capacitance C_{cryo} and the measurement of the potential difference ΔV between these electrodes: $C_{cryo} = Q/\Delta V$ [13, 50].

Considering the controlled number N of pumped electrons during a given period and the measurement of ΔV by comparison to the voltage of a Josephson device biased on n-th Shapiro step and irradiated at frequency f'_J, the capacitance is given by the relation

$$C_{cryo} = \big(N/nf'_J\big)K_J Q_X. \tag{17}$$

The capacitance C_{cryo} is then compared to a known capacitance C_X of a capacitor placed at room temperature. Two kinds of results could be obtained.

1) If C_X has been previously measured in terms of the second and R_K, by means of a complete measurement chain whose the keystone is a quadrature bridge enabling the impedance comparison between capacitance and resistance ($2\pi RCf_q = 1$ at equilibrium), it can be written in a simplified form as

$$C_X = A_1/\big(R_K f_q\big), \tag{18}$$

where A_1 is a dimensionless factor issued from the measurement and f_q is the balance frequency of the quadrature bridge. Combining the two last relations (17) and (18) leads to a new expression of the dimensionless product $R_K K_J Q_X$:

$$R_K K_J Q_X = A_1(n/N)(C_{cryo}/C_X)f'_J/f_q. \tag{19}$$

2) If the capacitance C_X has been directly compared to the capacitance variation ΔC of the Thompson-Lampard calculable capacitor ([2, 3] and references therein), and consequently known with a value expressed in SI units:

$$C_X = \{C_X\}_{SI}\mathrm{F} = A_2\{\Delta C\}_{SI}\mathrm{F}, \tag{20}$$

where the quantity inside brackets $\{\}_{SI}$ is a dimensionless numerical value and, using the same notation as before, A_2 is a dimensionless factor. Then, from relation (17) a SI value of the product $K_J Q_X$ can be deduced

$$K_J Q_X = A_2(N/n)(C_{cryo}/C_X)\big\{f_J\Delta C\big\}_{SI}\Omega^{-1} = A_3\big\{f'_J\Delta C\big\}_{SI}\Omega^{-1} \tag{21}$$

where $A_3 = A_2(N/n)(C_{\mathrm{cryo}}/C_{\mathrm{X}})$. Combining this SI determination of $K_{\mathrm{J}}Q_{\mathrm{X}}$ with the closure of the triangle *via* $U = RI$ leads to a new SI realisation of R_{K}

$$R_{\mathrm{K}} = A_4\{f_{\mathrm{SET}}\Delta C\}_{\mathrm{SI}}^{-1}\,\Omega, \tag{22}$$

where $A_4 = {A_3}^{-1}n(i/G_{\mathrm{CCC}})({f'}_{\mathrm{J}}/f_{\mathrm{J}})$. The two relations (21) and (22) give rise to measurements of a quantity whose value might be compared to the values of h/e^2 deduced from measurements in atomic physics (anomalous magnetic moment of electron, ground state hyperfine transition frequency of muonium, quotient of Planck constant and either relative atomic mass of cesium or neutron mass times lattice spacing of a crystal), or in solid state physics (shielded gyromagnetic ratio of proton). These provides new determinations of α if one assumes exact the relations $R_{\mathrm{K}} = h/e^2$, $K_{\mathrm{J}} = 2e/h$ and $Q_{\mathrm{X}} = e$. It is noteworthy that the first one is independent of QHE.

4˙2.3. Observational equations. It is thus shown that the QMT experiments do not consist solely in verifying the consistency of QHE, JE and SET. The closure of QMT *via* the two approaches $U = R \cdot I$ or $Q = C \cdot V$ might give significant information that can be taken into account in the adjustment periodically made on fundamental constants by the CODATA task group [8]. The adjustment is based on the method of least squares described in details by Mohr *et al.* in [51]. Using the same notation of the authors, the adjustment involves a large number of input data q_{i} (more than 80 in 2002), each of them being expressed as a function f_{i} of constants to be adjusted z_{i} (for example $\alpha, h, R_\infty, \ldots$) and giving rise to the set of observational equations.

$$q_{\mathrm{i}} \doteq f_{\mathrm{i}}(z_1, z_2, \ldots, z_{\mathrm{M}}). \tag{23}$$

The previous relations (16), (19), (21) and (22) correspond to new observational equations as follows [52]:

$$Q_{\text{X-90}} \doteq \big[\big(K_{\mathrm{J}}R_{\mathrm{K}}\big)/\big(K_{\text{J-90}}R_{\text{K-90}}\big)\big] \cdot [2\alpha h/(\mu_0 c)]^{1/2}, \tag{24}$$

$$K_{\mathrm{J}}Q_{\mathrm{X}} \doteq 4\alpha/(\mu_0 c), \tag{25}$$

$$R_{\mathrm{K}} \doteq \mu_0 c/(2\alpha), \tag{26}$$

where $Q_{\text{X-90}} = [I \times \mathrm{A}/\mathrm{A}_{90}]/f$, I is measured in conventional unit A_{90} and the assumptions $R_{\mathrm{K}} = h/e^2$ and $K_{\mathrm{J}} = 2e/h$ being relaxed.

4˙2.4. Determination of the elementary charge. It is noteworthy the great interest to combine all the three experiments, QMT, calculable capacitor and watt balance in a same laboratory or not. This would lead to a first direct determination of the quantum charge involved in SET devices, the expected electron charge, without assuming that $R_{\mathrm{K}} = h/e^2$ and $K_{\mathrm{J}} = 2e/h$. The best known value of e is at present the 2002 CODATA value ($e = 1.60217653\,\mathrm{C}$, with an uncertainty of 8.5 parts in 10^8) mainly issued from values of the Planck constant h (*via* watt balance) and the fine-structure constant α (g-2, h/m ratio and QHE).

The watt balance provides the SI value of the product $K_J{}^2 R_K$

$$K_J{}^2 R_K = A_5 \{ f_J{}^2/[Mgv] \}_{SI} \quad \Omega\,V^{-2}\,s^{-2}, \tag{27}$$

where, as before, A_5 is a dimensionless factor, f_J is the Josephson frequency. M, g and v correspond to the suspended mass, Earth's gravitational acceleration and the constant speed.

The determination of R_K from the complete experiment linking the Thompson-Lampard calculable capacitor to the quantum Hall resistance standard gives

$$R_K = A_6 \{ (\Delta C f_q)^{-1} \}_{SI}\,\Omega, \tag{28}$$

where A_6 is a dimensionless factor andf_q is the frequency of the balanced quadrature bridge.

These two experiments combined with QMT lead to the new observation equation

$$Q_X \doteq [2\alpha h/(\mu_0 c)]^{1/2}. \tag{29}$$

This relation can be deduced from (24) by considering that here the current I is measured in SI unit A. From the two approaches of QMT ($U = RI$ or $Q = CV$), the measured SI value of Q_X is given by

$$Q_X = A_7 \Big\{ \left[\Delta C f_q Mgv\right]^{1/2}/f_{SET} \Big\}_{SI}\,C, \tag{30}$$

or

$$Q_X = A_8 \Big\{ \left[\Delta C Mgv/f_q\right]^{1/2} \Big\}_{SI}\,C, \tag{31}$$

where A_7 and A_8 are dimensionless factors.

4˙3. *QMT experimental set-up using a CCC*

4˙3.1. Cryogenic current comparator (CCC). In general, the CCC is used in NMIs to calibrate resistances against quantum Hall resistance standards. This is the instrument which has allowed to demonstrate the universality of QHE with the highest accuracy. The CCC can also be used as a low-current amplifier with two characteristics never reached by any conventional device. The CCC may exhibit a current resolution around $1\,fA/Hz^{1/2}$ or less over the white-noise frequency range. This excellent resolution is mainly due to the low-noise properties of the magnetic flux detector used, currently a SQUID (Superconducting Quantum Interference Device) [53]. The second extraordinary feature of this cryogenic amplifier is the exactness of the current gain. The CCC is shortly described below. More details can be found in the literature [54].

The principle of CCC, invented by Harvey in 1972 [55], rests on Ampère's law and the perfect diamagnetism of the superconductor in the Meissner state. Given two wires

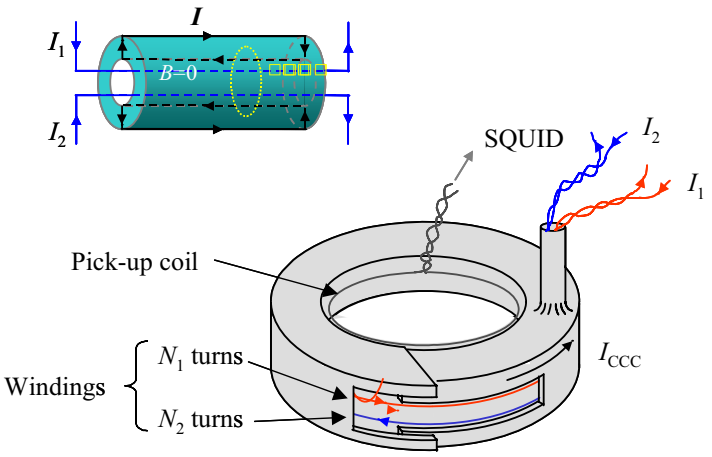

Fig. 14. – Toroidal structure of a CCC and principle (in insert). The supercurrent flowing up the inner surface of the toroidal shield is given by $I = N_1 I_1 + N_2 I_2$.

inserted in a superconducting tube (fig. 14), currents I_1 and I_2 circulating through these wires will induce a supercurrent I flowing up the inner surface of the tube and backing down the outer surface in such a way to maintain a null magnetic flux density B inside the tube.

Application of Ampère's law to a closed contour (a) in the bulk gives

$$\oint_a B \cdot \mathrm{d}l = 0 = \mu_0 \cdot (I_1 + I_2 - I) \tag{32}$$

and leads to the equality of the currents

$$I = I_1 + I_2. \tag{33}$$

If the tube contains N_1 and N_2 wires crossed, respectively, by currents I_1 and I_2, then (33) becomes

$$I = N_1 I_1 + N_2 I_2. \tag{34}$$

These equalities are valid independently of the position of the wires inside the tube. Here is the key reason of the high accuracy of the CCC. In practice, a CCC is made of two windings with N_1 and N_2 turns crossed by currents I_1 and I_2 circulating in opposite directions. These windings are enclosed in a superconducting torus [56], whose extremities overlap without being electrically connected on a length large enough to overcome the end effects, which distort the current equality in the real case of a finite length tube (fig. 14).

The outside magnetic flux Φ, which results only from the supercurrent I_{CCC}, is detected by a SQUID through a flux transformer composed of a pickup coil wound very close to the toroidal shield (on its inner or outer surface) and the input coil of the SQUID. The output voltage of the SQUID is then converted in a current, which feeds back one of the two windings to null the magnetomotive forces

$$N_1 I_1 - N_2 I_2 = 0. \tag{35}$$

From this ampere turn balance the equality of the ratios results

$$I_2/I_1 = N_1/N_2. \tag{36}$$

Except the case of a wrong number of turns in the windings, the error in the current ratio or equivalently in the current gain is in general very small, least measurable values of 10^{-11} having been reported so far. The ratio error comes mainly from a lack of efficiency of the superconducting toroidal shield (in a.c. measurements carried out at frequencies higher than 1 Hz, error sources arise from various capacitances inside the CCC).

The second relevant characteristic of the CCC is its current resolution δI_{CCC} in terms of $\mathrm{A/Hz^{1/2}}$ and is defined as the square root of the power spectral density of current noise referred to the CCC input, or equivalently as the minimum measurable supercurrent circulating in the overlapping tube of the CCC. The relation below gives a complete expression for δI_{CCC},

$$\delta I_{\mathrm{CCC}} = \left[4k_{\mathrm{B}}T/R_{\mathrm{in}} + 8\varepsilon/{N_1}^2 k^2 {L'}_{\mathrm{CCC}} + (S_{\Phi\mathrm{ext}}/N_1 {L'}_{\mathrm{CCC}})^2\right]^{1/2}, \tag{37}$$

where N_1 is the number of turns of the primary winding of the CCC, k is a coupling parameter between the pickup coil and the overlapping toroidal shield characterized by an effective inductance ${L'}_{\mathrm{CCC}}$ [54]. The first term corresponds to the Johnson noise of the input resistor R_{in} at temperature T. The second term is the contribution of the SQUID with an energy resolution ε when the optimal sensitivity of the CCC is reached. The third term comes from the external magnetic flux noise with a power spectral density $S_{\Phi\mathrm{ext}}$. This last term becomes negligible with careful shielding as described below. The dominant noise arises from one of the two first terms, depending on the CCC application. When a CCC is used for comparing resistance standards [6], the Johnson noise they deliver cannot be avoided and consequently the number of turns of the primary winding is increased to a limiting value (typically around 2000) above which the noise contribution of the SQUID becomes negligible. For low current measurements implying CCC-based current amplifier, very high input resistances are involved ($R_{\mathrm{in}} \gg 100\,\mathrm{M\Omega}$), and consequently only the SQUID noise contributes

$$\delta I_{\mathrm{CCC}} \approx \left[8\varepsilon/{N_1}^2 k^2 {L'}_{\mathrm{CCC}}\right]^{1/2}. \tag{38}$$

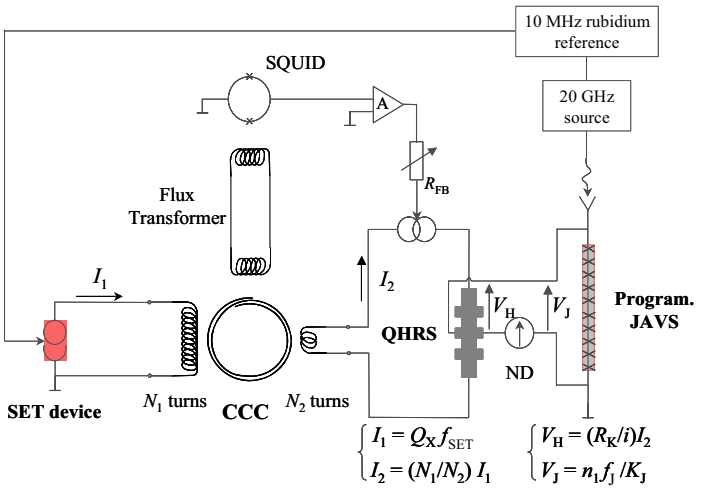

Fig. 15. – Basic circuit for closing the quantum metrological triangle.

4˙3.2. CCC used as a current amplifier. An experimental set-up for testing QMT is sketched in fig. 15. The current amplifier is composed of a CCC of high winding ratio, $G = N_1/N_2$, a d.c. SQUID with low white-noise level and low corner frequency f_c, and a secondary current source, servo controlled by the SQUID in such a way that the latter works at null magnetic flux and the relation (36) is verified [12]. In order to minimize the contribution from $1/f$ flicker noise, the polarity of the current to be amplified is periodically reversed. The Hall voltage is simultaneously compared to the voltage of a programmable Josephson junction array voltage standard (JAVS), well suited here because of the low voltage level and the requirement of periodic reversal of polarity [57]. The null detector will be balanced by adjusting the operating frequency of the SET source f_{SET}. This frequency and the irradiation frequency of the Josephson array are both referred to a 10 MHz rubidium clock.

The great challenge of this experiment is to reduce the type-A uncertainties to the level of few parts in 10^7 and ultimately one part in 10^8, taking into account the low current delivered by the SET source. The largest type-B uncertainties are estimated to be on the order of one part in 10^8 or less, and depend weakly on current level. They arise from the CCC ($u_{CCC} \approx 10^{-8}$ including capacitive leakage, finite open loop gain and winding ratio error), the quantum Hall resistance standard ($u_{QHRS} < 10^{-9}$ considering the effects of finite temperature, contact resistance and resistive leakage), the Josephson voltage set-up ($u_{JE} < 10^{-8}$ mainly due to residual e.m.f., resistive leakage, detector and frequency error) and the SET experimental set-up ($u_{SET} < 10^{-9}$ coming from current leakage and frequency error) without taking into account intrinsic errors of SET device (missing events due to pumping frequency, cotunneling and thermal effects).

In order to analyze the different noise sources and to estimate the possible type-A uncertainties, let us consider a simplified diagram of the QMT experiment as shown

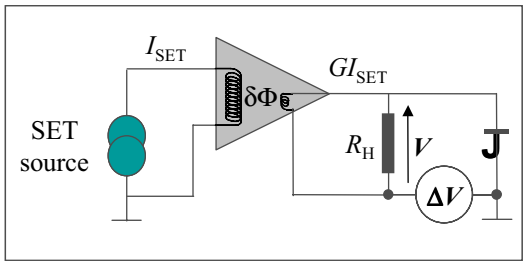

Fig. 16. – Principle of a QMT experiment involving a CCC-based current amplifier.

in fig. 16. Two detectors are used: the SQUID which detects the magnetic flux $\delta\Phi$ induced by the supercurrent in the CCC and to be zeroed, and a voltmeter to measure the deviation ΔV between the Hall and Josephson voltages.

The voltage noise recorded by the voltmeter and referred to the nominal voltage V is given by the expression

$$\delta V/V = \left[\delta I^2{}_{\mathrm{CCC}} + 4k_{\mathrm{B}}T/G^2R_{\mathrm{H}} + \left(\delta V^2{}_{\mathrm{ND}} + \delta V^2{}_{\mathrm{emf}}\right)/G^2R^2{}_{\mathrm{H}}\right]^{1/2}/I_{\mathrm{SET}}, \tag{39}$$

where one finds again in the first term the current resolution of the CCC directly linked to magnetic flux noise $\delta\Phi$ at the SQUID input. The second term reflects the Johnson noise of the quantum Hall resistance, while the third term corresponds to the noise generated by the null detector (ND) itself including the instability of unwanted electromotive forces.

The required CCC for amplifying the very small current generated by the SET source must present high winding ratio and ultra low noise performances. In this framework, some CCCs with winding ratios from 10 000:1 to 109 999:1 have been investigated by NMIs [58-63]. They present input current noise $\delta I_{\mathrm{CCC}}|_{\mathrm{exp}}$ from 0.8 to 4 fA/Hz$^{1/2}$ in the white-noise range (typically $f > 0.1$ Hz) although measured in the favourable case where the CCC was not connected to SET device. The input current noise undoubtedly increases once the input winding of the CCC is connected to a SET current source (due to increased influence of antenna loop effects, microphonics effects). For example, δI_{CCC} has been found in the order of 12 fA/Hz$^{1/2}$ with a CCC connected to an electron pump compared to the initial value 4 fA/Hz$^{1/2}$ [64]. All The experimental values $\delta I_{\mathrm{CCC}}|_{\mathrm{exp}}$ are around ten times higher than the expected values $\delta I^2{}_{\mathrm{CCC}}|_{\mathrm{theo}}$ varying from 80 to 700 aA/Hz$^{1/2}$. Some improvements have thus to be done for reducing this margin and a value of 1 fA/Hz$^{1/2}$ might be considered as a first reasonable target.

The Johnson noise term is made negligible by designing CCC with a gain higher than 10^4. Considering a QHE sample cooled at current temperature of 1.3 K and operating on the $i = 2$ resistance plateau ($R_{\mathrm{H}}(i = 2) = R_{\mathrm{K}}/2 \approx 13\,\mathrm{k}\Omega$), the term $(4k_{\mathrm{B}}T/G^2R_{\mathrm{H}})^{1/2}$ is only in the order of 7 aA/Hz$^{1/2}$.

The null detector generates both noise voltage δU_{ND} and noise current δI_{ND}. The latter depends on the resistance placed at the input of the detector and might become dom-

inant if a threshold resistance value is exceeded. The last term of relation (39) can then be expressed by

$$(40)\quad \big(\delta V^2{}_{\mathrm{ND}} + \delta V^2{}_{\mathrm{e.m.f.}}\big)/G^2R^2{}_{\mathrm{H}} = \big(\delta U^2{}_{\mathrm{ND}} + \delta V^2{}_{\mathrm{e.m.f.}}\big)/G^2R^2{}_{\mathrm{H}} + \delta I^2{}_{\mathrm{ND}}(R_{\mathrm{H}})/G^2.$$

Considering the previous case with $G = 10^4$ and $R_{\mathrm{H}} \approx 13\,\mathrm{k\Omega}$, the noise characteristics $\delta I_{\mathrm{ND}} \approx 100\,\mathrm{fA/Hz^{1/2}}$ and $\delta U_{\mathrm{ND}} \approx 20\,\mathrm{pV/Hz^{1/2}}$ (corresponding to an equivalent noise resistance of $40\,\Omega$) of the EM model N11 nanovoltmeter and $\delta V_{\mathrm{e.m.f.}} \approx 1\,\mathrm{nV/Hz^{1/2}}$ typically, it results

$$\big[\big(\delta V^2{}_{\mathrm{ND}} + \delta V^2{}_{\mathrm{e.m.f.}}\big)/G^2R^2{}_{\mathrm{H}}\big]^{1/2} \approx 14\,\mathrm{aA/Hz^{1/2}}.$$

This value is well below the CCC current resolution.

With the target value of $1\,\mathrm{fA/Hz^{1/2}}$ for δI_{CCC}, the total noise detected by the voltmeter and referred to the input voltage might amount to $\delta V/V \approx 1 \times 10^{-3}/\mathrm{Hz^{1/2}}$ for a current of 1 pA.

Finally, the experimental standard deviation of the mean for a set of data can be estimated, either with a power spectral density calculus either with an Allan deviation one [65,66]. These calculi can be carried out only if the noise is white. In this case, $s(\bar{I})$ represents the type-A uncertainty associated to the mean value of the current $\bar{I}$ [67] and the Allan deviation is an unbiased estimator of $s(\bar{I})$ [65,66].

$$(41)\quad s\big(\bar{I}\big)/\bar{I} = [h_0 f_0/(2N)]^{1/2},$$

where h_0 ($= \delta V^2 \cdot \bar{I}/V^2$) is the white-noise level (in $\mathrm{A^2/Hz}$) as defined in [66], f_0 is the sampling frequency of the measurement and N is the total number of values.

The condition of white noise will be fulfilled if the current to be measured is periodically reversed at a frequency slightly higher than the corner frequency f_{C} of the SQUID. f_{C} defines the frontier between the domains of $1/f$ noise and white noise. In fig. 17 we report a typical set of data over a measurement time T_{N} and composed of N reversals of current. f_{M} denotes the modulation frequency of a single measurement (two current reversals) and n the number of values per trace taken with an integrating frequency f_{i} : $f_{\mathrm{M}} = f_{\mathrm{i}}/n$, $T_{\mathrm{N}} = N/f_{\mathrm{M}}$.

The sampling frequency to be considered is equal to the frequency f_M and consequently

$$s\big(\bar{I}\big)/\bar{I} = [h_0 f_{\mathrm{M}}/(2N)]^{1/2},$$

or

$$(42)\quad s\big(\bar{I}\big)/\bar{I} = [h_0/(2T_{\mathrm{N}})]^{1/2}.$$

For $h_0^{1/2} = 1\,\mathrm{fA/Hz^{1/2}}$ and considering the typical values used at LNE [24], $f_{\mathrm{M}} = 0.14\,\mathrm{Hz}$, the experimental standard deviation of the mean $s(\bar{I})$ from a one-hour measurement

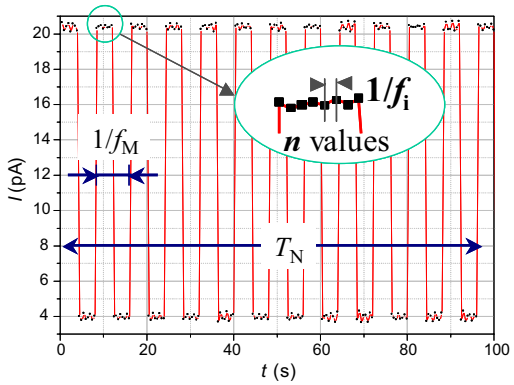

Fig. 17. – Set of values recorded at the output of the SQUID of the CCC during a measurement carried out at LNE. The current delivered by an electron pump is periodically reversed at a frequency so that the SQUID works in the white-noise regime.

would amount to 10 aA, *i.e.* around 7.4 parts in 10^6 for a current of 1.6 pA delivered by an electron pump operating at 10 MHz. This is already lower than the uncertainties obtained for the same current amplitude with the best conventional bridge (involving integration method) so far.

With the system at LNE, using a CCC in non-optimal working mode([3]) (the SQUID being flux-locked by feeding the current to its modulation coil and not to the secondary winding of the CCC), the current of 16 pA generated by an electron pump at 100 MHz has been measured with a type A uncertainty of 55 aA (*i.e.* a relative uncertainty of 3.5 parts in 10^6) after 6.5 hours of measurement [64] in agreement with ${h_0}^{1/2}$ measured at the level of 12 fA/Hz$^{1/2}$. From this result, some improvements have to be made both on R pump and CCC used as current amplifier to reach an uncertainty below one part in 10^6. SET devices capable to supply currents up to 100 pA and generating lower noise must be developed in order to attempt the ultimate uncertainty of 1 part in 10^8. A new amplifier with a better sensitivity is also needed. This can be obtained by increasing the CCC gain with a factor 5 and by using a SQUID well suited to the experiment.

4˙3.3. CCC used both in the calibration of a cryogenic resistance and as current detector. The principle of QMT experiment implying a CCC as a current detector instead of a current amplifier is sketched on fig. 18. It presents the advantage of involving a single detector with a very low input current noise and allowing current reversals faster than in the previous case, *i.e.* at frequencies of 1 Hz or higher [48], thus operating the SQUID far from the $1/f$ noise regime.

([3]) *i.e.* in an internal feedback mode, where the SQUID is flux-locked by feeding the current to its modulation coil and not to the secondary winding of the CCC.

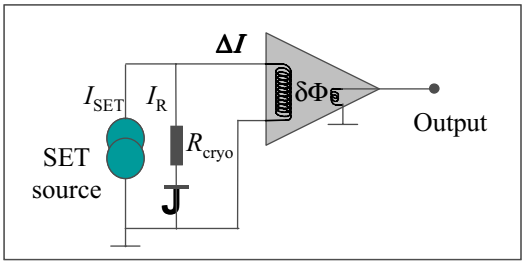

Fig. 18. – Principle of a QMT experiment with a CCC operating as a SQUID ammeter, the primary winding being the input coil coupled to the SQUID via a flux transformer. Induced by a voltage generated by a Josephson array to a cryogenic resistor, a current I_R is opposed to a current I_{SET} delivered by a SET device.

The expected value of the type-A uncertainty on the current deviation $\Delta I = I_{SET} - I_R$ will be given by

$$s(\bar{I})/\bar{I} = (\delta I/\bar{I})/{T_N}^{1/2} \tag{43}$$

with

$$\delta I = \left(4k_B T/R_{cryo} + {\delta I^2}_{CCC}\right)^{1/2} \tag{44}$$

by taking into account the intrinsic current noise of the CCC given by the relation (38). A cryogenic resistor of 100 MΩ, as proposed at NIST [48], cooled down to 1.3 K (in a simple pumped helium bath) generates a current noise of about 800 aA/$\mathrm{Hz}^{1/2}$, in the same order of the noise of the null detector described in 5.2.2. making the two approaches equivalent in terms of type-A uncertainties which could be reached.

In this experiment the challenge to overcome is the calibration of the cryogenic resistance, whose value of 100 MΩ has to be measured in terms of R_K with an uncertainty as low as one part in 10^8. This requires a specific CCC bridge enabling a direct comparison with QHR [49].

4˙4. *QMT experimental set-up using an electron counting capacitance standard.* – The QMT has been successfully closed within an uncertainty of one part in 10^6 at NIST [50]. As shown in fig. 19, the system consists of a seven junctions electron pump, a SET transistor/electrometer with a charge detection threshold of the order of $e/100$, and a cryogenic capacitor of 1.8 pF capacitance. Two mechanical cryogenic switches N_1 and N_2 allow two working phases:

a) *N_1 closed, N_2 open*

In this phase, the cryogenic capacitance C_{cryo} (≈ 1 pF) is charged with N electrons generated one by one through the pump. The process is stopped for a short time (20 s) to measure the voltage ${V_c}^+$. Then, the pump is forced to transfer N electrons in the opposite

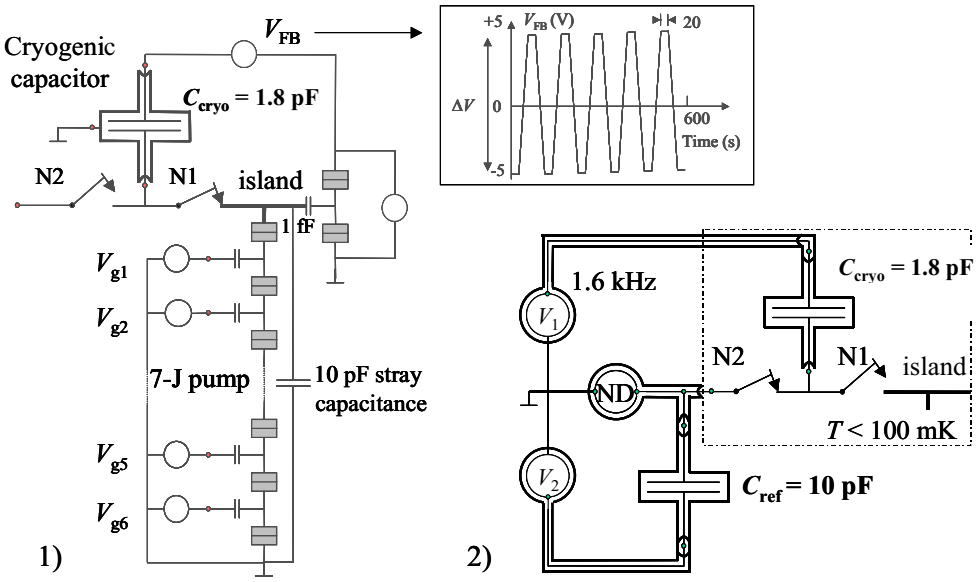

Fig. 19. – Principle of electron counting capacitance standard [50]. Two operating modes: 1) N_1 closed, N_2 open: electrons are periodically pumped forward and backward, 2) N_1 open, N_2 closed: The cryogenic capacitance is compared to a reference capacitance.

direction. Another stop occurs to measure a voltage V_c^-, and so on. The successive voltages V_c^+ and V_c^- are compared to those of a JAVS and the differences $\Delta V = V_c^+ - V_c^-$ are calculated. The average of these differences $\langle \Delta V \rangle$ gives the capacitance

$$C_{\text{cryo}} = Ne/\langle \Delta V \rangle = \big(N/nf_J\big) K_J Q_X \tag{45}$$

from the relation $\langle \Delta V \rangle = nf_J/K_J$, where n is the index of the voltage step provided by the binary Josephson array at a frequency f_J.

b) *N_1 open, N_2 closed*

In this second configuration, C_{cryo} is compared with the capacitance C_x of a capacitor at room temperature using a capacitance bridge. This capacitance comparison is carried out at a frequency in the kHz range, much higher than the effective frequency of electron counting (25 mHz) and at 15 V of rms voltage value (compared to 3.5 V in the first phase).

Keller *et al.* [68] has recently established a complete uncertainty budget on the results reported in 1999 [50]. The combined total uncertainty amounts to around 9.5 parts in 10^7 and mainly results from the uncertainty components given below.

For the electron counting phase, the relative standard deviation of C_{cryo} values is in the order of 1.4 to 2.4 parts in 10^7 depending on the run performed (three runs in total). The type-A uncertainties lie within 1.2 and 2.3 parts in 10^7 while the two most important type-B uncertainties amount to 5 parts in 10^8 and 4 parts in 10^8 corresponding to the calibration of the digital voltmeter against JAVS and the capacitive leakage of

C_{cryo}, respectively. About the electron pumping error, earlier measurements have shown uncertainties of one part in 10^8 at frequencies of a few MHz [22].

For the capacitance comparison phase, the commercial bridge used was traceable to the calculable capacitance standard at NIST with a calibration uncertainty of 8.5 parts in 10^7. This corresponds to the most important type-B uncertainty, the other are in the order of 2 parts in 10^7 (for example the correction of cable loading effects), while the type-A uncertainty here has been found ten times lower.

Last but not least, type-B uncertainties corresponding to the frequency and voltage dependences of the cryogenic capacitance have to be taken into account. They amount to 2 parts in 10^7 [69] and 9 parts in 10^8 [68], respectively.

Unlike the $U = RI$ approach, this experiment does not need a SET source supplying currents higher than a few pA to close the triangle at least with an uncertainty of one part in 10^7. This uncertainty level will be reached by this method if efforts are undertaken particularly on the capacitance measurement. A drastic improvement will be in implementing a coaxial capacitance bridge based on two terminal-pair method [70]. This will be absolutely required in order to reduce more the uncertainty and to reach the level of few parts in 10^8. This also needs a better knowledge of the frequency dependence of the cryogenic capacitor. Presently the observed logarithmic increase of the capacitance when the frequency decreases below few 100 Hz might be due to dielectric dispersion and dissipation of insulating films of Cu_2O formed on the surface of the electrodes [69].

Within this frame, developments of ECCS are also in progress at other NMIs. A cryogenic capacitor with highly symmetrical coaxial electrode arrangement has been developed at the PTB: $C_{\mathrm{cryo}} = 1.435\,\mathrm{pF}$ at 4.2 K, drift $< 1\,10^{-7}$/day when the capacitor is maintained at low temperature, $\Delta C_{\mathrm{cryo}}/C_{\mathrm{cryo}} = 1.3\,10^{-6}$ during several thermal cycling [71]. In addition to the highly reliable cryogenic switches, METAS has designed and fabricated a tuned capacitor [72]. The capacitance value can be adjusted at room temperature so that the value is equal to the nominal value 1 pF within 3 parts in 10^5 allowing to take advantage of high-precision capacitance bridges.

5. – Conclusion and prospects

The development of the Coulomb blockade nanodevices opens extended prospects for applications in fundamental electrical metrology, *i.e.* the development of current and capacitance standards, and, more crucially, the closure of the quantum-metrological triangle and the determination of the elementary charge. These experiments could contribute to establish a new frame of the SI, fully based on fundamental constants by creating a direct link between the fundamental physics and the units. The target uncertainty needs to be around few parts in 10^7 and then ultimately one part in 10^8. If there is no deviation, our confidence on the three phenomena to provide us with $2e/h$, h/e^2 and e will be considerably enhanced. Any significant discrepancy will prompt further experimental and theoretical work. The closure of the quantum-metrology triangle, at these required uncertainties, should be assisted by improvements in new SET devices which could generate accurate currents as high as 100 pA. Ideas currently under investigation for the

implementation of a higher-frequency-locked current source include improved R-pumps, silicon-based electron pumps, SETSAW devices, superconducting Cooper pair pumps as a generalization of a single electron pump, Cooper pair sluices, Bloch oscillation devices, *etc.* Efforts have also to be pursued and encouraged in the improvement of CCCs, cryogenic capacitors and associated measurement techniques.

The Coulomb blockade nanodevices also present a high metrological potential in the applied domain in electricity and ionising radiation (calibration of sub-nano ammeters and development of charge detector), in thermometry (absolute cryogenic thermometer with so-called Coulomb blockade thermometer invented by Pekola *et al.* [73] and commercially available), in nanometrology (nanometer scale displacement sensor) and in new fields based on single-photon sources (single- or multiple-photon discrimination metrology, quantum cryptography and computing). Moreover some encouraging preliminary results and the advances in nanofabrication techniques (miniaturization of the tunnel junctions) will improve the performances of SET devices and allow them to operate at higher temperatures in future.

All these emerging applications in addition to those reaching maturity in fundamental electrical metrology (quantum standards based on QHE samples arrays and Josephson junctions arrays) and in time and frequency domain (microwave frequency standards by cooling atoms, femtosecond optical frequency combs, ion optical clocks ...) give signs on the metrology of the future, a science more and more focused on the measurement of discrete quantities rather than continuous quantities by detecting, manipulating, counting elementary entities (electron or charge quantum, flux quantum, photon ...). This evolution explains the present discussion around the new formulation of the SI which should express more our present knowledge on quantum physics and the date of its implementing will mark this crossover.

REFERENCES

[1] Kovalevsky J. and Quinn T. J., *C. R. Phys.* **5** (2004).
[2] Thompson A. M. and Lampard D. G., *Nature*, **177** (1956) 888.
[3] Trapon G., Thévenot O., Lacueille J. C. and Poirier W., *Metrologia*, **40** (2003) 159.
[4] Von Klitzing K., Dorda G. and Pepper M., *Phys. Rev. Let.*, **45** (1980) 494.
[5] Prange R. E. and Girvin S. M. (Editors), *The Quantum Hall Effect* (Springer-Verlag, New York) 1990.
[6] Jeckelmann B and Jeanneret B., this volume, p. 135.
[7] Josephson B. D., *Phys. Lett.*, **1** (1962) 251.
[8] Mohr P. J. and Taylor B. N., *Rev. Mod. Phys.*, **77** (2005) 1.
[9] Kibble B. P., in *Atomic Masses and Fundamental constants 5*, edited by Sanders J. H. and Wapstra A. H. (Plenum, New York) 1976, pp. 545-551.
[10] Genevès G. *et al.*, *IEEE Trans. Instrum. Meas.*, **54** (2005) 850.
[11] Likharev K. and Zorin A., *J. Low Temp. Phys.*, **59** (1985) 347.
[12] Piquemal F. and Genevès G., *Metrologia*, **37** (2000) 207.
[13] Williams E. R., Ghosh R. N. and Martinis J. M., *J. Res. Natl. Stand. Technol.*, **97** (1992) 299.

[14] AVERIN D. V. and LIKHAREV K. K., in *Mesoscopic Phenomena in Solids*, edited by AL'TSHULER B. I., LEE P. A. and WEBB R. A. (Elsevier, Amsterdam) 1990, p. 173.
[15] GRABERT H. and DEVORET M. H. (Editors), *Single Charge Tunneling: Coulomb Blockade Phenomena in Nanostructures* (Plenum Press, New York) 1992.
[16] LIKHAREV K. K., *Proc. IEEE*, **87** (1999) 606.
[17] ZELLER H. R. and GIAVER I., *Phys. Rev.*, **181** (1969) 789.
[18] POTHIER H. *et al.*, *Europhys. Lett.*, **17** (1992) 249.
[19] FELTIN N., DEVOILLE L., PIQUEMAL F., LOTKHOV S. and ZORIN A., *IEEE Trans. Instrum. Meas.*, **52** (2003) 599.
[20] KELLER M. W., MARTINIS J. M., STEINBACH A. H and ZIMMERMAN N. M., *IEEE Trans. Instrum. Meas.*, **46** (1997) 307.
[21] JENSEN H. D. and MARTINIS J. M., *Phys. Rev. B*, **46** (1992) 13407.
[22] KELLER M. W., MARTINIS J. M., ZIMMERMAN N. M and STEINBACH A. H, *Appl. Phys. Lett.*, **69** (1996) 1804.
[23] LOTKHOV S. V., BOGOSLOVSKY S. A., ZORIN A. B. and NIEMEYER J., *Appl. Phys. Lett.*, **78** (2001) 946.
[24] STECK B. *et al.*, *CPEM Digest* (2006) 158.
[25] BRENNING H., KAFANOV S., DUTY T., KUBATKIN S. and DELSING P., *J. Appl. Phys.*, **100** (2006) 114321.
[26] SCHOELKOPF R. J., WAHLGREN P., KOZHEVNIKOV A. A., DELSING P. and PROBER D. E., *Science*, **280** (1998) 1238.
[27] BYLANDER J. *et al.*, *Nature*, **434** (2005) 361.
[28] SHILTON J. M. *et al.*, *J. Phys.: Condens. Matter*, **8** (1996) L531.
[29] EBBECKE J., FLETCHER N. E., AHLERS F. J., HARTLAND A. and JANSSEN T. J. B. M., *IEEE Trans. Instrum. Meas.*, **52** (2003) 594.
[30] FLETCHER N. E., JANSSEN T. J. B. M. and HARTLAND A., *BEMC Digest* (2001).
[31] FLETCHER N. E. *et al.*, *Phys. Rev. B*, **68** (2003) 245310.
[32] ALHERS F. J., KIELER O. F. O., SAGOL B. E., PIERZ K. and SIEGNER U., *CPEM Digest* (2006) 154.
[33] LEEK P. *et al.*, *Phys. Rev. Lett.*, **95** (2005) 256802-1.
[34] SHIN YUN-SOK *et al.*, *CPEM Digest* (2006) 228.
[35] GEERLIGS L. J. *et al.*, *Z. Phys. B*, **85** (1991) 349.
[36] ZORIN A. B., BOGOSLOVSKY S. A., LOTKHOV S. V. and NIEMEYER J., Cond-mat/0012177 (2000).
[37] NISKANEN A. O., PEKOLA J. P. and SEPPÄ H., *Phys. Rev. Lett.*, **91** (2003) 177003/1.
[38] KEMPPINEN A. *et al.*, *CPEM Digest* (2006) 164.
[39] HAVILAND D. B., KUZMIN L. S., DELSING P., LIKHAREV K. K. and CLAESON T., *Z. Phys. B: Condens. Matter*, **85** (1991) 339.
[40] BOULANT N. *et al.*, Cond-mat/0605061 (2006).
[41] LOTKHOV S. V., KRUPENIN V. A. and ZORIN A. B., *CPEM Digest* (2006) 166.
[42] GALLOP J. C., *Philos. Trans. R. Soc. London, Ser. A*, **363** (2005) 2221.
[43] FUJIWARA A., ZIMMERMAN N. M., ONO Y. and TAKAHASHI Y., *Appl. Phys. Lett.*, **84** (2004) 1323.
[44] TSAI J. S., JAIN A. K. and LUKENS J. E., *Phys. Rev. Lett.*, **51** (1983) 316.
[45] HARTLAND A., JONES K., WILLIAMS J. M., GALLAGHER B. L. and GALLOWAY T., *Phys. Rev. Lett.*, **66** (1991) 969.
[46] JECKELMANN B., INGLIS A. D. and JEANNERET B., *IEEE Trans. Instrum. Meas.*, **44** (1995) 269.
[47] MOHR P. J., NEWELL D. B. and TAYLOR B. N., private communication (2006).

[48] Elmquist R., Zimmerman N. M. and Huber W. H., *IEEE Trans. Instrum. Meas.*, **52** (2003) 590.
[49] Elmquist R. E., Hourdakis E., Jarret D. G. and Zimmerman N. M., *IEEE Trans. Instrum Meas.*, **54** (2005) 525.
[50] Keller M. W., Eichenberger A. L., Martinis J. M. and Zimmerman N. M, *Science*, **285** (1999) 1706.
[51] Mohr P. J. and Taylor B. N, *J. Phys. Chem. Ref. Data*, **28** (1999) 1713.
[52] Piquemal F. *et al.*, *C. R. Physique*, **5** (2004) 857.
[53] Clarke J. and Braginski A. I. (Editors), *The SQUID Handbook*, Vol. **I** and Vol. **II** (WILEY-VCH Verlag GmbH&Co.FgaA, Weinheim), 2004-2006.
[54] Gallop J. C. and Piquemal F., chapter 9 in *The SQUID Handbook Vol. **II***, edited by Clarke J. and Braginski A. I. (WILEY-VCH Verlag GmbH&Co.FgaA, Weinheim) 2006, pp. 95-137.
[55] Harvey I. K., *Rev. Sci. Instrum.*, **43** (1972) 1626.
[56] Sullivan D. B. and Dziuba R. F., *Rev. Sci. Instrum.*, **45** (1974) 517.
[57] Hamilton C. A., Burroughs C. J. and Kautz R. L., *IEEE Trans. Instrum. Meas.*, **44** (1995) 223.
[58] Hartland A., *BEMC Digest* (1993) 18/1.
[59] Janssen T. B. J. M. and Hartland A., *Phys. B.*, **284-288** (2000) 1790.
[60] Gay F., Piquemal F. and Genevès G., *Rev. Sci. Instrum.*, **71** (2000) 4592.
[61] Gay F., PhD Thesis, Conservatoire National des Arts et Métiers, Paris, France (2000).
[62] Bartolomé E., PhD Thesis, Twente University, The Netherlands (2002).
[63] Rietveld G. *et al.*, *IEEE Trans. Instrum. Meas.*, **52** (2003) 621.
[64] Steck B. *et al.*, to be submitted to *Metrologia* (2007).
[65] Allan D. W., *IEEE Trans. Instrum. Meas.*, **36** (1987) 646.
[66] Witt T., *IEEE Trans. Instrum. Meas.*, vol. **50** (2001) 445.
[67] *Guide to the Expression of Uncertainty in Measurement*, International Standardization Organisation (ISO), ISBN 92-67-10188-9 (1993).
[68] Keller M. W. and Zimmerman N. M., to be submitted to *Metrologia* (2007).
[69] Zimmerman N. M., Simonds B. J. and Wang Y., *Metrologia*, **43** (2006) 383.
[70] Kibble B. P and Rayner G. H., *Coaxial AC bridges*, edited by Bailey A. E. (Adam Hilger Ltd., Bristol) 1984.
[71] Willemberg G. D. and Warnecke P., *IEEE Trans. Instrum. Meas.*, **50** (2001) 235.
[72] Overney F., Jeanneret B. and Furlan M., *IEEE Trans. Instrum. Meas.*, **49** (2000) 1326.
[73] Pekola J. K., Hirvi K. P., Kauppinen J. P. and Paalanen M. A., *Phys. Rev. Lett.*, **73** (1994) 2903.